Towards deterministic downscaling of SMOS soil moisture using MODIS derived soil evaporative efficiency

Olivier Merlin, J.P. Walker, Ghani Chehbouni, Yann H. Kerr

Towards deterministic downscaling of SMOS soil moisture using MODIS derived soil evaporative efficiency

Olivier Merlin [a,*], Jeffrey P. Walker [a], Abdelghani Chehbouni [b], Yann Kerr [b]

[a] Civil and Environmental Engineering, The University of Melbourne, Australia
[b] Centre d'Etudes Spatiales de la Biosphère (CESBIO), Toulouse, France

ARTICLE INFO

ABSTRACT

A deterministic approach for downscaling ~40 km resolution Soil Moisture and Ocean Salinity (SMOS) observations is developed from 1 km resolution MODerate resolution Imaging Spectroradiometer (MODIS) data. To account for the lower soil moisture sensitivity of MODIS surface temperature compared to that of L-band brightness temperature, the disaggregation scale is fixed to 10 times the spatial resolution of MODIS thermal data (10 km). Four different analytic downscaling relationships are derived from MODIS and physically-based model predictions of soil evaporative efficiency. The four downscaling algorithms differ with regards to i) the assumed relationship (linear or nonlinear) between soil evaporative efficiency and near-surface soil moisture, and ii) the scale at which soil parameters are available (40 km or 10 km). The 1 km resolution airborne L-band brightness temperature from the National Airborne Field Experiment 2006 (NAFE'06) are used to generate a time series of eleven clear sky 40 km by 60 km near-surface soil moisture observations to represent SMOS pixels across the three-week experiment. The overall root mean square difference between downscaled and observed soil moisture varies between 1.4% v/v and 1.8% v/v depending on the downscaling algorithm used, with soil moisture values ranging from 0 to 15% v/v. The accuracy and robustness of the downscaling algorithms are discussed in terms of their assumptions and applicability to SMOS.

1. Introduction

Soil moisture observations over large areas are increasingly required in a range of environmental applications including meteorology, hydrology, water resource management and climatology. Various approaches have been developed over the past two decades to infer near-surface soil moisture from remote sensing measurements of surface temperature, radar backscatter and microwave brightness temperature (e.g. Prigent et al., 2005; Crow and Zhan, 2007). The relative merit of these approaches depends on i) the strength of the physical link between the observable in the different spectral domains and soil water content, and ii) the spatial/temporal resolution that is technically achievable by the different spaceborne remote sensing systems. The physical link between L-band brightness temperature and soil moisture profile (up to 5 cm) has been shown to be stronger than at higher frequency, and more direct than with radar backscatter and with thermal data (Kerr, 2007; Wagner et al., 2007).

The Soil Moisture and Ocean Salinity (SMOS) mission (Kerr et al., 2001) is to be the first soil moisture dedicated satellite. It will use L-band radiometry to provide data of the 0–5 cm soil moisture every 3 days at 40 km resolution globally. Despite the high sensitivity of passive microwave radiometers to near-surface soil moisture, their spatial resolution is about 10 to 500 times coarser than that of active microwave and optical systems. For instance, the L-band Phased Array type L-band Synthetic Aperture Radar (PALSAR) and the Advanced Spaceborne Thermal Emission and Reflection Radiometer (ASTER) can achieve a spatial resolution of about 100 m. Note however that current and planned radar observations have repeat cycles of about 30 days with high-resolution products and about 6 days with medium-resolution products such as 1 km resolution C-band Advanced Synthetic Aperture Radar (ASAR) data. In the optical domain, high-resolution data are also currently acquired sparsely with a repeat cycle of 16 days for ASTER. In fact, only optical sensors at intermediate spatial resolution, such as the MODerate resolution Imaging Spectroradiometer (MODIS) having 1 km resolution, provide a global coverage every 1–2 days.

Given the high soil moisture sensitivity but low spatial resolution of passive microwave data, and the high spatial resolution but non-optimal soil moisture sensitivity of optical/thermal data, the combination of both types of information is expected to result in reliable soil moisture products at intermediate spatial resolution. However, such downscaling approaches need to be matured so that SMOS data can be used in the numerous applications requiring high-resolution soil moisture information. To date, disaggregation strategies based on optical data have been developed by building either stochastic (e.g.

* Corresponding author. Tel.: +61 3 8344 5628.
E-mail addresses: omerlin@unimelb.edu.au, merlin@cesbio.cnes.fr (O. Merlin).
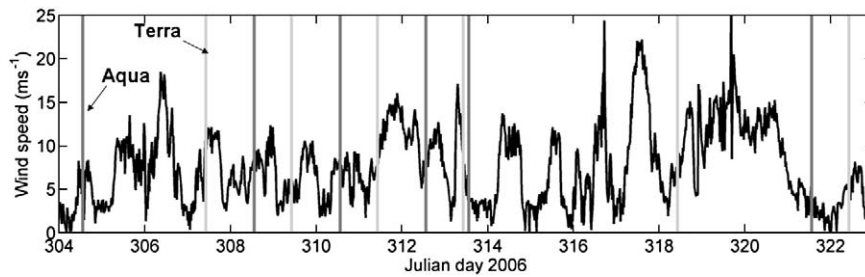
Fig. 1. Time series of wind speed monitored at Y11 in the Yanco area. The overpass time on clear sky days of MODIS/Terra (10 am) and MODIS/Aqua (1 pm) are also shown.

Chauhan et al., 2003) or deterministic (e.g. Merlin et al., 2006b) relationships between near-surface soil moisture and optical-derived soil moisture indices. While stochastic approaches have the advantage of requiring few ancillary data, they may not be valid outside the conditions used for calibration. Conversely, deterministic approaches can potentially be transferred to a wider range of conditions, but generally require a larger amount of surface parameters and micro-meteorological data which may not be available over large areas.

This paper develops a novel analytic approach for downscaling ~40 km resolution SMOS soil moisture from 1 km resolution MODIS derived and physically-based model predictions of soil evaporative efficiency (soil evaporative efficiency is defined as the ratio of the actual to potential soil evaporation). Four different downscaling algorithms are developed, differing only in i) the assumed relationship (linear or nonlinear) between soil evaporative efficiency and near-surface soil moisture and ii) the scale at which soil parameters are available (40 km or disaggregation scale). The four algorithms are tested with data from the National Airborne Field Experiment 2006 (NAFE'06, Merlin et al., 2008b). A simulated SMOS near-surface soil moisture observation is derived from the Polarimetric L-band Multi-beam Radiometer (PLMR) data acquired at 1 km resolution over the 40 by 60 km Yanco area on eleven cloud free days during the three-week campaign. Moreover, the 1 km resolution data are also used to verify downscaling results at the disaggregation scale. The downscaling algorithms are compared in terms of accuracy and robustness with the NAFE'06 data set. Their operational applicability to SMOS is also discussed.

2. Data

NAFE'06 was undertaken from 30 October to 20 November 2006 in the Murrubidgee catchment, in southeastern Australia. A detailed description of the data set is provided in Merlin et al. (2008b) so only the pertinent details are given here. The data used in this study are composed of: the 1 km resolution PLMR data over the 40 by 60 km Yanco area, the MODIS data acquired over the Yanco area on clear sky days during the three-week experiment, and a times series of wind speed measurements at one micro-meteorological station included in the study area.

2.1. L-band derived soil moisture

During NAFE'06, L-band brightness temperature was mapped at 1 km resolution over the 40 by 60 km Yanco area on 11 days: JD 304, 306, 307, 308, 309, 311, 313, 317, 318, 320 and 322. A soil moisture product at 1 km resolution was derived over the area from PLMR data on each acquisition date (Merlin et al., submitted for publication). The error in soil moisture retrievals as compared to ground measurements aggregated to 1 km resolution was estimated to be less than 4% v/v. Note that the presence of standing water over rice crops included in the Yanco area was not explicitly accounted for in the retrieval procedure. By doing so, all water surfaces were interpreted as bare soil with 100% moisture content. In other words, any standing water in the

1 km PLMR pixels systematically increases the retrieved soil moisture. However, this assumption is consistent with the use of MODIS surface temperature and NDVI to estimate soil evaporative efficiency (see next section).

2.2. MODIS data

The MODIS data used in the downscaling algorithms are composed of MODIS/Terra (10 am) and MODIS/Aqua (1 pm) 1 km resolution daily surface temperature, and MODIS/Terra 1 km resolution 16-day Normalized Difference Vegetation Index (NDVI). The MODIS NDVI data are from Terra only to minimize sun-glint effects occuring with Aqua reflectances at lower sun incidence angles. The 16-day NDVI product was cloud free. In between the first (Julian day JD 304) and last day (JD 322) of 1 km resolution PLMR flights over Yanco, 12 MODIS surface temperature images with less than 10% cloud cover were acquired including six aboard Terra (JD 307, 309, 311, 313, 318 and 322) and six aboard Aqua (JD 304, 308, 310, 312, 313 and 321).

2.3. Wind speed data

Wind speed was monitored at 2 m by a meteorological station near Y11 (southwestern corner of the Yanco area) continuously during NAFE'06 with a time step of 20 minutes. The time series is illustrated in Fig. 1. Note that wind speed is assumed to be uniform within the 40 by 60 km area, at the time of MODIS overpass.

3. Approach

The three general steps of the downscaling approach consist of (i) estimate soil evaporative efficiency from MODIS data (ii) link soil evaporative efficiency to near-surface soil moisture via a physically-based scaling function and (iii) build a downscaling relationship to express high-resolution near-surface soil moisture as function of SMOS-scale observation and high-resolution soil evaporative efficiency.

3.1. MODIS-derived soil evaporative efficiency

The fine-scale information used in the downscaling procedure is the soil evaporative efficiency derived from MODIS surface temperature and MODIS NDVI. The rationale for choosing soil evaporative efficiency as fine-scale information is based on the strong correlation with near-surface soil moisture (Anderson et al., 2007) and its relative stability during daytime on clear sky days (Shuttleworth et al., 1989; Nichols and Cuenca, 1993; Crago and Brutsaert, 1996). The soil evaporative efficiency β is estimated as in Nishida et al. (2003).

$$\beta_{MODIS} = \frac{T_{max} - T_{MODIS}}{T_{max} - T_{min}} \qquad (1)$$

with T_{max} being the soil temperature at minimum soil moisture, T_{min} the soil temperature at maximum soil moisture, and T_{MODIS} the soil

Table 1
Model parameters

Parameter	Value	Unit	Source
θ_{c0}	2.5	% v/v	Default value estimated from Komatsu (2003)
γ	100	s m^{-1}	Default value estimated from Komatsu (2003)
z_{0m}	0.005	m	Typical value for bare soil Liu et al. (2007)
$NDVI_{min}$	0.22	–	Estimated from NDVI image
$NDVI_{max}$	0.60	–	Estimated from NDVI image

skin temperature derived from MODIS data at the time of interest. Using the triangle approach (Price, 1980; Carlson et al., 1995), T_{MODIS} can be expressed as

$$T_{MODIS} = \frac{T_{surf, MODIS} - f_{veg} T_{veg}}{1 - f_{veg}} \qquad (2)$$

with $T_{surf,MODIS}$ being the MODIS surface skin temperature, T_{veg} the vegetation skin temperature and f_{veg} the vegetational fraction cover. Herein, T_{MODIS} is defined as the temperature of the bare soil when vegetation temperature T_{veg} is assumed to be uniform within the SMOS pixel. In this formulation of soil evaporative efficiency, the impact of spatially variable root-zone soil moisture on T_{veg} is not accounted for. Note that β varies between 0 and 1 when $f_{veg} < 1$ and is not defined when $f_{veg} = 1$. Cover fraction is computed as

$$f_{veg} = \frac{NDVI_{MODIS} - NDVI_{min}}{NDVI_{max} - NDVI_{min}} \qquad (3)$$

with $NDVI_{MODIS}$ being the MODIS observed NDVI, and $NDVI_{min}$ and $NDVI_{max}$ the minimum and maximum NDVI values for a particular scene.

Five parameters are needed to compute soil evaporative efficiency from MODIS data: $NDVI_{min}$, $NDVI_{max}$, T_{veg}, T_{min} and T_{max}. While $NDVI_{min}$ and $NDVI_{max}$ are assumed to be constant within the Yanco area during NAFE'06, T_{veg}, T_{min} and T_{max} are assumed to be uniform within the Yanco area, but vary in time. Parameters $NDVI_{min}$ and $NDVI_{max}$ are determined from the 16-day NDVI product within the SMOS pixel. Vegetation temperature T_{veg} is estimated at the time of overpass (10 am or 1 pm) as the minimum temperature reached at maximum NDVI ($f_{veg} = 1$). Minimum temperature T_{min} can be estimated either over fully vegetated pixels by assuming $T_{min} \sim T_{veg}$ or over water bodies as the minimum temperature reached at minimum NDVI. Parameter T_{max} is the value extrapolated along the dry edge of the triangle. As the impact of root-zone soil moisture on T_{veg} is neglected, the dry edge is interpreted as the 1 km pixels with dry soils in the near-surface. Note that the accuracy in extrapolating T_{max} depends on moisture conditions within the study area; it is optimum in dry-end conditions and is expected to be relatively low in uniformly wet conditions.

3.2. Scaling function

Although evaporative fraction has been shown to be relatively constant between 10 am and 1 pm (MODIS overpass times), several studies have indicated that it cannot be considered as completely independent from atmospheric conditions (Lhomme and Elguero, 1999; Gentine et al., 2007). Moreover, in constant soil moisture and atmospheric conditions, soil evaporative efficiency may significantly vary with soil type (Komatsu, 2003). To account for these temporal (atmospheric) and spatial (atmospheric and soil properties) effects, the MODIS-derived β computed from Eq. (1) is explicitly linked to near-surface soil moisture θ by the following model from Komatsu (2003)

$$\beta_{model} = 1 - \exp(-\theta/\theta_c) \qquad (4)$$

with $\theta_c = \theta_{c0}(1 + \gamma/r_{ah})$, θ_{c0} (% v/v) and γ (s m^{-1}) being two soil-dependent parameters and r_{ah} (s m^{-1}) the aerodynamic resistance over bare soil, given the soil roughness z_{0m} (see Table 1) and the wind speed u at a reference height (2 m in our case). Komatsu's model was validated over bare soil for the very top soil layer (1 mm). The empirical parameter θ_{c0} (typical range 1–4% v/v) controls the soil capacity to retain moisture in optimal evaporative conditions i.e. when wind speed is zero or r_{ah} is infinite. In other words, the higher θ_{c0}, the slower the soil dries.

By inverting the soil evaporative efficiency model from Eq. (4), one obtains:

$$\theta_{model} = -\theta_c \ln(1 - \beta) \qquad (5)$$

This model provides an estimate of the slope of the correlation between near-surface soil moisture and soil evaporative efficiency, $\partial \theta_{model}/\partial \beta = \theta_c/(1-\beta)$ and an estimate of the "non-linearity" of this correlation, $\partial^2 \theta_{model}/\partial \beta^2 = \theta_c/(1-\beta)^2$. Note that the non-linearity of θ_{model} is a decreasing function of near-surface soil moisture and is maximum at $\beta = 0$.

3.3. Downscaling relationships

The physically-based model of Eq. (4) is used to derive four deterministic relationships between downscaled soil moisture, simulated SMOS observations, and MODIS-derived soil evaporative efficiency.

3.3.1. Linear approximation

A downscaling relationship is derived by writing the first-order Taylor series approximation of the downscaled soil moisture θ at the SMOS-scale observation θ_{SMOS}

$$\theta = \theta_{SMOS} + \left(\frac{\partial \theta}{\partial \beta}\right) \Delta \beta_{MODIS} \qquad (6)$$

with $\Delta \beta_{MODIS}$ being the difference between MODIS-derived soil evaporative efficiency and its integrated value at the SMOS scale. As in the recent study of Merlin et al. (2008a), the function $f_1 = \partial \theta/\partial \beta$ is used to convert β variations into soil moisture variations about the low-resolution observation. The main difference here is that this function f_1 depends on soil type, wind speed, and SMOS-scale near-surface soil moisture. In Merlin et al. (2008a), the function f_1 was assumed to be constant and was estimated during a training period. Herein, the simple model of Eq. (4) requiring two soil parameters (θ_{c0} and γ) and wind speed is used to describe explicitly the variability of the relationship between soil evaporative efficiency and near-surface soil moisture for different soils, wind speed and moisture conditions at the SMOS scale. Note that Eq. (6) relies on the assumption that the 0–1 mm soil moisture (as described by MODIS evaporative efficiency) and the 0–5 cm soil moisture (as derived from PLMR brightness temperature) have the same spatial variability about the mean within the SMOS pixel.

By replacing f_1 by its analytical expression, the downscaling relationship of Eq. (6) becomes

$$\theta = \theta_{SMOS} + \theta_c \frac{\Delta \beta_{MODIS}}{1 - \beta_{SMOS}} \qquad (7)$$

with $\beta_{SMOS} = \int \partial \beta/\partial \theta \, d\theta$ the integral of β at the SMOS scale. Eq. (7) can be simplified as

$$\theta = \theta_{SMOS} + \theta_c SMP_{MODIS} \qquad (8)$$

with SMP_{MODIS} a soil moisture proxy defined as

$$SMP_{MODIS} = \frac{\Delta \beta_{MODIS}}{1 - \beta_{SMOS}} \qquad (9)$$

By assuming that (i) T_{max} and T_{min} are mostly uniform within the SMOS pixel and (ii) the integral $T_{SMOS} = \int \partial T / \partial \theta \, d\theta$ is approximately equal to the areal average of T_{MODIS}, SMP can be computed as

$$SMP_{MODIS} = \frac{T_{SMOS} - T_{MODIS}}{T_{MODIS} - T_{min}} \qquad (10)$$

The major advantage of this formulation over Eq. (9) is that SMP does not depend on the soil temperature at minimum soil moisture T_{max}.

3.3.2. Second-order correction

A second downscaling relationship is derived by adding the term in β^2 in the Taylor series expansion:

$$\theta = \theta_{SMOS} + \left(\frac{\partial \theta}{\partial \beta}\right) \Delta \beta_{MODIS} + \frac{1}{2}\left(\frac{\partial^2 \theta}{\partial \beta^2}\right) \Delta \beta_{MODIS}^2 \qquad (11)$$

Note that f_1 is now θ-dependent. In particular, the second derivative $\partial^2 \theta / \partial \beta^2$ specifically accounts for the non-linear relationship between soil evaporative efficiency and near-surface soil moisture at about θ_{SMOS}.

By replacing the first and second derivatives with their analytical expression, the downscaling relationship of Eq. (11) becomes

$$\theta = \theta_{SMOS} + \theta_c \left[\frac{\Delta \beta_{MODIS}}{1 - \beta_{SMOS}} + \frac{\Delta \beta_{MODIS}^2}{2(1 - \beta_{SMOS})^2}\right] \qquad (12)$$

and after simplification

$$\theta = \theta_{SMOS} + \theta_c \left(SMP_{MODIS} + \frac{1}{2}SMP_{MODIS}^2\right) \qquad (13)$$

with SMP_{MODIS} defined as in Eq. (10).

3.3.3. Downscaling relationships

Four downscaling relationships are derived from Eqs. (8) and (13). They differ with regards to their degree of complexity by assuming a linear (or non-linear) relationship between soil evaporative efficiency and near-surface soil moisture, and by using soil parameter θ_c estimated at low- (or high-) resolution:

- Downscaling scheme D1 is based on the linear approximation between β and θ, and assumes θ_c is uniform:

$$D1 : \theta = \theta_{SMOS} + \theta_{c,SMOS} SMP_{MODIS} \qquad (14)$$

- Downscaling scheme D2 includes a second-order correction in SMP_{MODIS}^2, and assumes θ_c is uniform:

$$D2 : \theta = \theta_{SMOS} + \theta_{c,SMOS}\left(SMP_{MODIS} + \frac{1}{2}SMP_{MODIS}^2\right) \qquad (15)$$

- Downscaling scheme D1′ is based on the linear approximation between β and θ, and accounts for the variability of θ_c at the downscaling resolution:

$$D1' : \theta = \theta_{SMOS} + \theta_{c,MODIS} SMP_{MODIS} \qquad (16)$$

- Downscaling scheme D2′ includes a second-order correction in SMP_{MODIS}^2, and accounts for the variability of θ_c at the scale of the downscaling resolution:

$$D2' : \theta = \theta_{SMOS} + \theta_{c,MODIS}\left(SMP_{MODIS} + \frac{1}{2}SMP_{MODIS}^2\right) \qquad (17)$$

Note that the difference between D1 and D1′, and likewise the difference between D2 and D2′, is simply the spatial scale at which soil parameters are estimated.

4. Application

The four downscaling algorithms of Eqs. (14)–(17) are tested with the NAFE'06 data set. The "goodness" of the disaggregation process is measured by two estimators: the root mean square difference and the correlation coefficient between 10 km resolution disaggregated soil moisture and 10 km resolution L-band retrieval.

4.1. Validation approach

The approach for verification of downscaling results is illustrated in Fig. 2. The 1 km resolution L-band derived soil moisture is
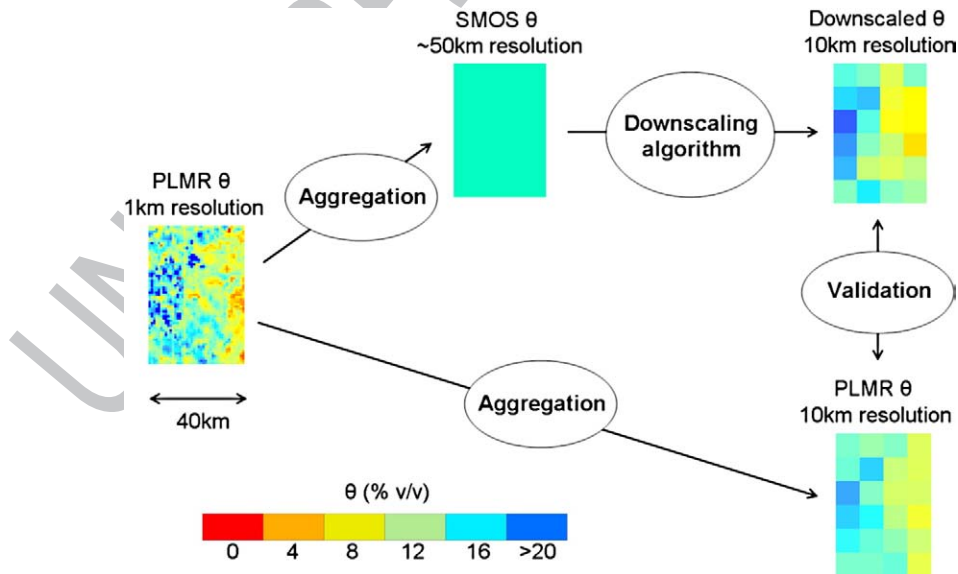

Fig. 2. Schematic diagram of the validation approach. Downscaling results are validated at 10 km resolution to account for the lower sensitivity (relative to PLMR data) of MODIS surface temperature to near-surface soil moisture.

Table 2
List of the acquisition date of MODIS data, satellite platform (Aqua/1 pm and Terra/10 am), minimum soil temperature T_{min}, wind speed u, SMOS-scale soil moisture θ_{SMOS}, and its variability (standard deviation) at 1 km resolution σ_{SMOS}

		T_{min}	u	θ_{SMOS} (σ_{SMOS})
Day	Satellite	°C	ms^{-1}	% v/v
304	Aqua	37	6	4.4 (4.9)
307	Terra	28	10	16.6 (5.4)
308	Aqua	37	5	11.0 (4.6)
309	Terra	35	8	6.5 (4.6)
310	Aqua	38	8	5.4 (4.5)[a]
311	Terra	33	9	4.2 (4.4)
312	Aqua	35	7	4.0 (4.3)[a]
313	Terra	32	8	3.8 (4.3)
313	Aqua	39	4	3.8 (4.3)
318	Terra	27	6	11.3 (3.8)
321	Aqua	37	5	8.0 (4.6)[a]
322	Terra	37	6	5.4 (4.7)
All[b]	Terra	33	7	6.2 (4.4)
All	Aqua	37	6	6.1 (4.5)

[a] Interpolated between dates.
[b] All dates except 307.

aggregated over the 40 by 60 km Yanco area to generate a ~40 km resolution SMOS type soil moisture observation on each PLMR flight day. The time series of θ_{SMOS} and its sub-pixel variability at 1 km resolution σ_{SMOS} are presented in Table 2. The simulated SMOS resolution observation ranges from 4 to 17% v/v with a spatial variability at 1 km resolution of about 5% v/v. These coarse observations are next disaggregated at higher spatial resolution using 1 km resolution daily MODIS-derived SMP. The L-band derived soil moisture product is then used to verify downscaling results at the disaggregation scale.

In this study, the disaggregation scale is 10 km. Consequently, the MODIS-derived soil temperature is aggregated from 1 km to 10 km to derive SMP at 10 km resolution. There are several rationales for aggregating MODIS-derived soil temperature. First, the aggregation of MODIS derived SMP to 10 km is expected to increase the sensitivity of SMP to near-surface soil moisture (the sensitivity of surface temperature to near-surface soil moisture is relatively low compared to that of L-band brightness temperature). Second, the aggregation limits the errors on downscaled results associated with the presence of clouds in surface temperature images and with the re-sampling strategy that is required for comparison with gridded PLMR data. Third, meteorological forcing (wind speed notably) reacts to the surface heterogeneity in an organized manner at scales larger than 1 km (Shuttleworth et al., 1997).

The four algorithms of Eqs. (14)–(17) are applied to 12 MODIS surface temperature images and downscaling results are compared to the PLMR retrieval aggregated to 10 km resolution on the same grid as MODIS derived SMP. For the three MODIS overpass days (JD 310, 312, and 321) on which no PLMR flight was undertaken, PLMR data are interpolated between dates by averaging soil moisture products obtained on the day before and day after. The interpolation is valid because no rainfall occurred during the period.

4.2. MODIS derived SMP

All downscaling relationships in (14)–(17) are based on the MODIS derived SMP computed from the soil temperature T_{MODIS} and the minimum soil temperature T_{min}. The MODIS-derived soil temperature is computed by estimating T_{veg} for each MODIS surface temperature image. Fig. 3 presents the triangles obtained by plotting 1 km resolution MODIS surface temperature (Terra or Aqua) against 1 km resolution NDVI (16-day product from Terra platform). The vegetation temperature is estimated as the minimum surface temperature reached at maximum NDVI (0.6). The MODIS-derived SMP is then computed by estimating T_{min} for each MODIS surface temperature image. In practice, the minimum soil temperature is approximated to the vegetation temperature
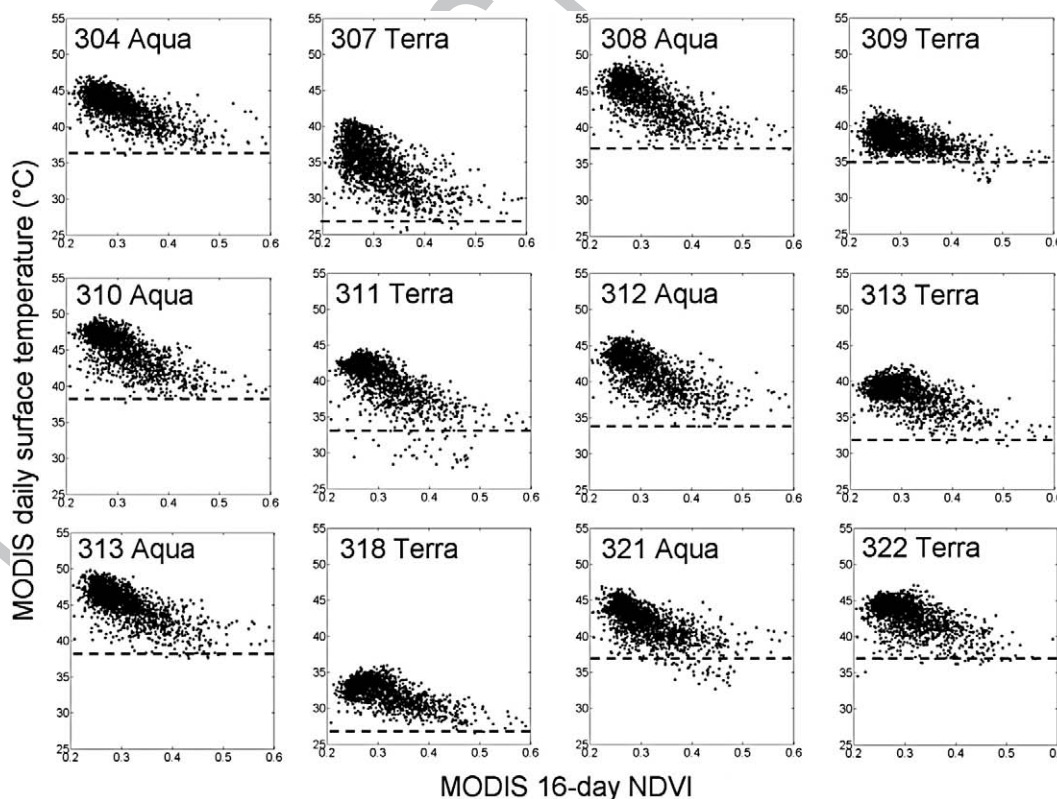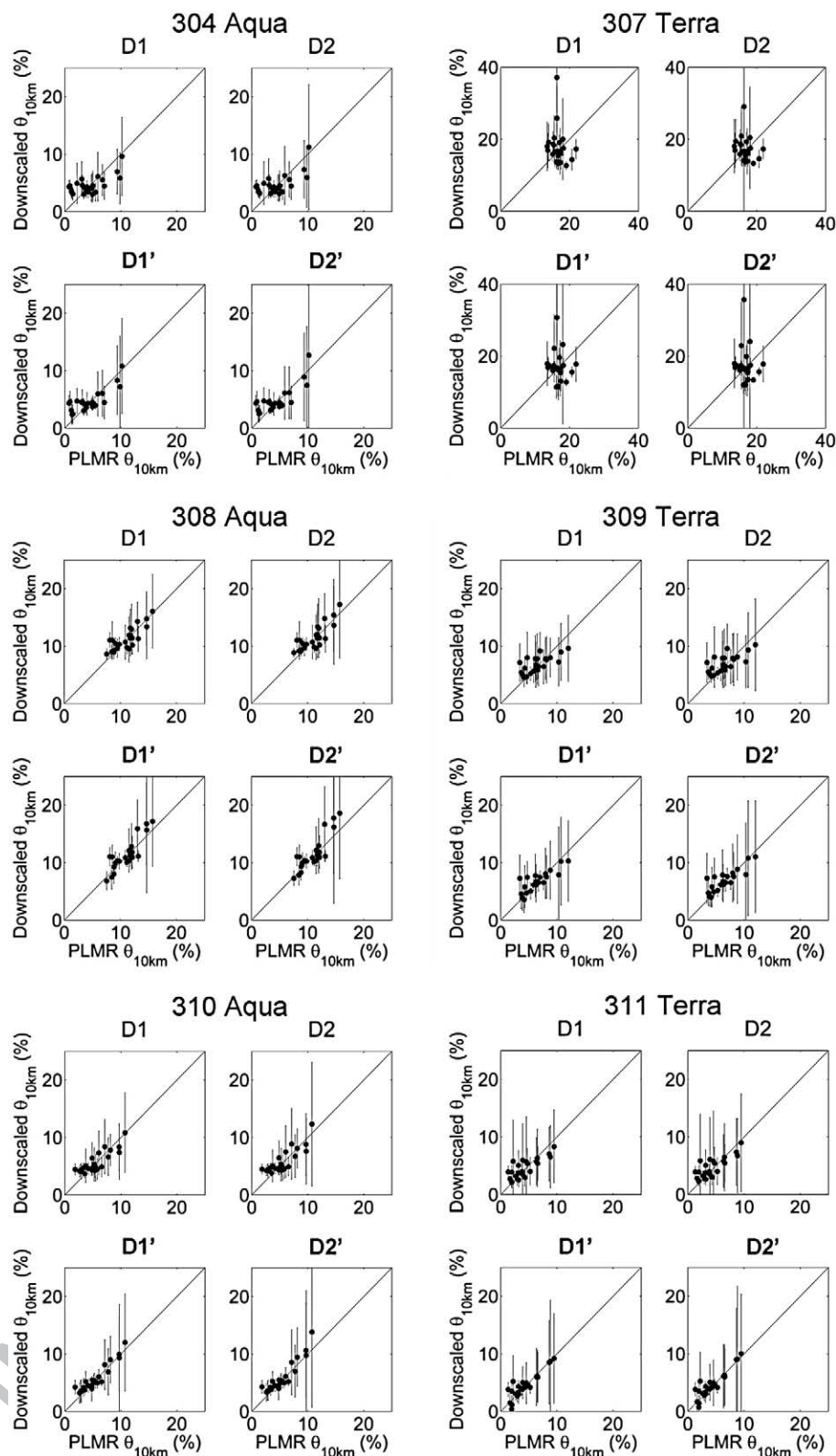

Fig. 3. MODIS daily surface temperature versus MODIS 16-day NDVI. The minimum soil temperature (and vegetation temperature) is represented in dash line.

Fig. 4. Downscaled versus PLMR derived soil moisture for each clear sky MODIS surface temperature image between JD 304 and 311. Results include the downscaled soil moisture at 10 km resolution (circles), and its sub-pixel variability (error bars).

$T_{min} = T_{veg}$. One physical explanation behind this is that both vegetation temperature and the soil temperature at saturation are in first approximation close to the air temperature. Note that on JD 311 and 321, the surface temperature of some pixels is below the vegetation temperature. This can be explained by the presence of small clouds on the images and/or a de-coupling between soil skin temperature with evaporation. However, this effect was relatively small, and did not appear on the other days. Parameter T_{min} is listed in Table 2 for each of the 12 MODIS surface temperature images.
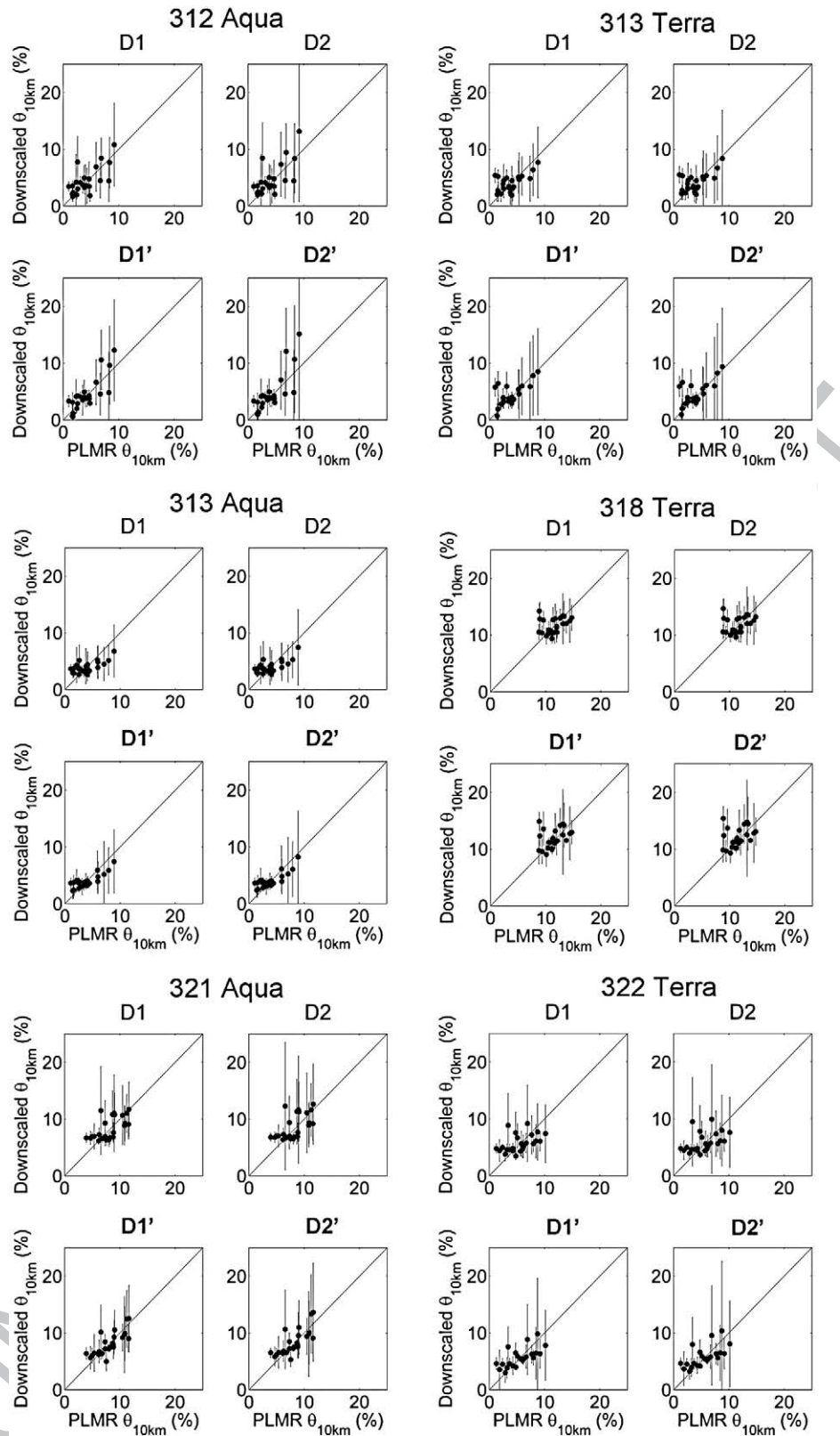
Fig. 5. As for Fig. Fig. 4 but between JD 312 and 322.

4.3. Downscaling with D1 and D2 (uniform θ_c)

Downscaling schemes D1 and D2 are applied to the NAFE'06 data set. In Eqs. (14) and (15), parameter $\theta_{c,SMOS}$ is evaluated by estimating θ_{c0} and γ when the soil type is not known. In Komatsu (2003), θ_{c0} varied from 1 % v/v for sand to 4 % v/v for agricultural (clay) soil, and γ varied from 85 to 115 s m^{-1}. Herein, default values are fixed to θ_{c0}=2.5% v/v and γ=100 s m^{-1}.

Downscaling results are presented in Figs. 4 and 5 for each MODIS image separately. The data points represent the 10 km resolution

Table 3
List of the acquisition date of MODIS data, satellite platform (Aqua/1 pm and Terra/10 am), root mean square error (RMSE) on the 10 km resolution downscaled soil moisture θ, and the correlation coefficient R^2 between 10 km resolution downscaled and PLMR derived soil moisture

		RMSE on $\theta_{10\ km}$				Correlation coefficient R^2			
		D1	D2	D1′	D2′	D1	D2	D1′	D2′
Day	Satellite	% v/v	%v/v	% v/v	% v/v	–	–	–	–
304	Aqua	2.0	2.0	1.6	1.7	0.67	0.67	0.81	0.79
307	Terra	5.7	8.6	7.0	11	−0.18	−0.13	−0.08	−0.07
308	Aqua	1.3	1.4	1.4	1.6	0.82	0.82	0.86	0.85
309	Terra	1.6	1.6	1.3	1.3	0.69	0.70	0.82	0.84
310	Aqua	1.3[a]	1.5[a]	0.85[a]	1.1[a]	0.85[a]	0.84[a]	0.93[a]	0.92[a]
311	Terra	1.4	1.4	1.0	1.0	0.79	0.80	0.90	0.91
312	Aqua	1.8[a]	2.1[a]	1.6[a]	2.1[a]	0.68[a]	0.68[a]	0.81[a]	0.80[a]
313	Terra	1.6	1.6	1.6	1.7	0.62	0.64	0.68	0.69
313	Aqua	1.6	1.6	1.3	1.2	0.70	0.71	0.85	0.84
318	Terra	1.8	1.9	1.9	2.0	0.29	0.27	0.35	0.33
321	Aqua	1.9[a]	2.0[a]	1.4[a]	1.6[a]	0.61[a]	0.60[a]	0.77[a]	0.75[a]
322	Terra	2.2	2.3	1.8	1.8	0.47	0.43	0.68	0.64
All[b]	Terra	1.7	1.8	1.5	1.6	0.57	0.57	0.68	0.68
All	Aqua	1.6	1.7	1.4	1.6	0.72	0.72	0.84	0.83

[a] PLMR data interpolated between dates.
[b] All dates except 307.

Fig. 6. Downscaling results at 10 km resolution obtained on all acquisition dates except JD 307.

downscaled soil moisture $\theta_{10\ km}$ and the errorbars represent the 1 km variability in 10 km fields $\sigma_{10\ km}$, computed as the standard deviation of downscaled θ at 1 km resolution. Quantitative results in terms of root mean square error (RMSE) and correlation coefficient with L-band derived soil moisture are presented in Table 3. The downscaled soil moisture is generally in good agreement with PLMR retrieval with an overall RMSE of 1.7% v/v and 1.8% v/v for D1 and D2 respectively, and an overall correlation coefficient of about 0.7 for both schemes.

On JD 307 however, the correlation coefficient is negative (−0.2) for both D1 and D2 and the RMSE is 6% v/v and 8% v/v for D1 and D2 respectively. In particular, the RMSE is higher in both cases than the variability of 1 km resolution L-band derived soil moisture within the SMOS pixel (σ_{SMOS}=5% v/v), which means that the ~40 km resolution observation is a better estimate of near-surface soil moisture than the downscaled one at scales ranging from 1 km to 40 km. Those poor results are probably due to the poor estimates of L-band derived soil moisture on this particular day. The relationship between MODIS surface temperature and NDVI in Fig. 3 obtained on JD307 is consistent with that obtained on the other days. Consequently, MODIS surface temperature on JD307 can reliably be used to derive SMP. The point is that the MODIS surface temperature image on JD 307 is the only image available that directly follows one of the two major rainfall events of NAFE'06. In particular, the rainfall event during the night of JD 306–307 might be the cause of a temporary change in vegetation water content or possibly intercepted water (Merlin et al., 2008b), resulting in an unreliable L-band derived soil moisture product. Independently from the impact of canopy water storage on microwave soil moisture retrieval, one should note that the disaggregation approaches will not operate well in very wet conditions, under which surface skin temperature is generally de-coupled from soil moisture levels. This de-coupling is due to a switch from moisture-limited (dry) to energy-limited (wet) conditions.

The comparison between schemes D1 and D2 shows that better results in terms of RMSE and correlation coefficient are generally obtained with the linear approximation (D1). The inclusion of a second-order correction slightly deteriorates the results. It is argued that the agregation of the MODIS derived soil temperature and L-band derived soil moisture from 1 km to 10 km tends to "linearize" the relationship between soil evaporative efficiency and soil moisture. The aggregation to 10 km makes the linear approximation approach more valid than the second-order correction one. Moreover, the simple model of Eq. (4) does not 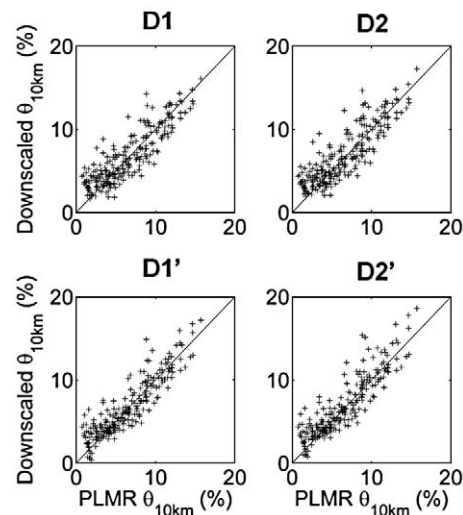represent the saturation of soil evaporative efficiency at very low soil moisture values as modelled in Sellers et al. (1992). This saturation is visible in Fig. 6 for soil moisture values below 5% v/v.

4.4. Downscaling with D1′ and D2′ (spatially variable θ_c)

The variability of soil type within the SMOS pixel is now accounted for in the disaggregation scheme. Soil parameter θ_c is first fitted with MODIS SMP and PLMR soil moisture retrieval during a calibration period JD 304–311. The $\theta_{c,MODIS}$ values at 10 km resolution are then used in the application of downscaling schemes D1′ and D2′ to the whole period JD 304–322.

Parameter θ_c is a function of two soil-dependent parameters θ_{c0} and γ. In Komatsu (2003), γ and θ_{c0} were estimated for three different substrates (sand, agricultural soil, and cornstarch). In that study, most of the variability in θ_c was attributed to θ_{c0} (1% v/v for sand and 4% v/v for clay), while γ remained relatively constant. To simplify our analysis, parameter γ is thus fixed to a constant, estimated from the average of the values in Komatsu (2003) (γ=100 s m^{-1}). This approximation is consistent with the relatively high uncertainty in wind speed associated with the extrapolation of point-measurements (meteorological station) to the 40 by 60 km Yanco area.
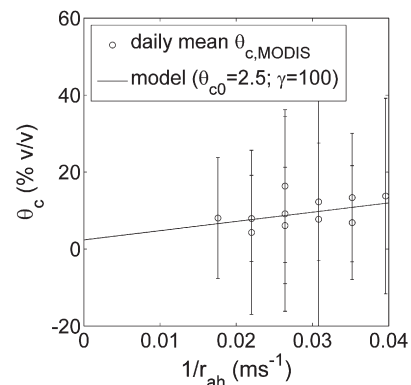

Fig. 7. Areal average (circle) and spatial variability (error bar) within the SMOS pixel of MODIS retrieved $\theta_{c,MODIS}$ versus $1/r_{ah}$. The aerodynamic resistance r_{ah} was computed from ground-based measurements of wind speed. Modelled θ_c is also plotted for comparison.
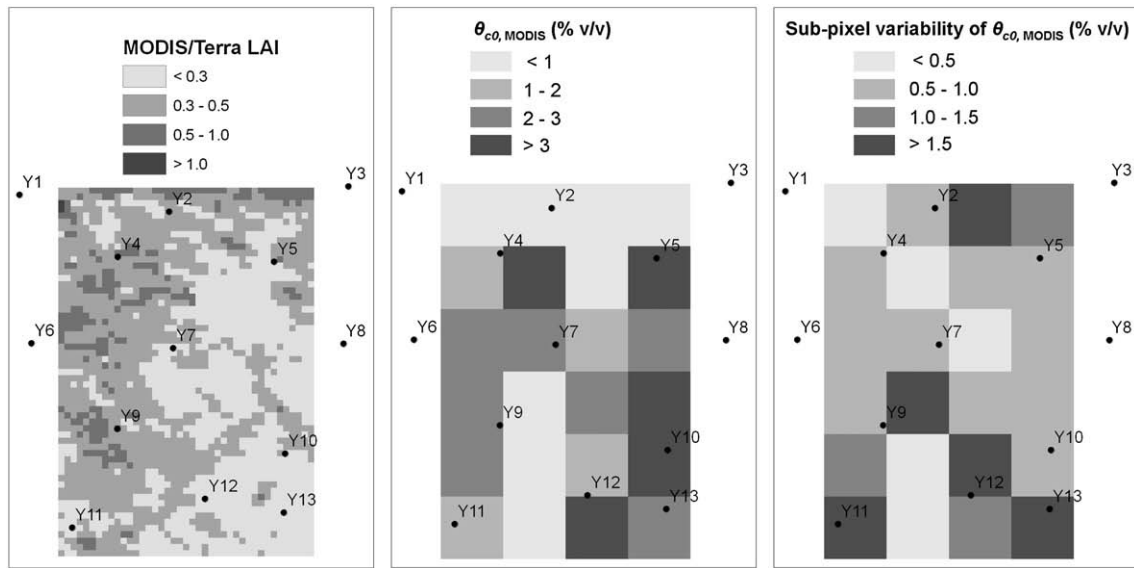
Fig. 8. Map over the 40 by 60 km Yanco area of 1 km resolution MODIS/Terra LAI (left), the retrieved 10 km resolution $\theta_{c0,\text{MODIS}}$ (centre) and its sub-pixel variability (right).

Given downscaling scheme D1 was found to be more accurate than downscaling scheme D2, Eq. (16) is used to estimate parameter $\theta_{c,\text{MODIS}}$:

$$\theta_{c,\text{MODIS}} = \frac{\theta_{\text{PLMR}} - \theta_{\text{SMOS}}}{\text{SMP}_{\text{MODIS}}} \qquad (18)$$

from L-band derived soil moisture θ_{PLMR} and MODIS derived SMP using the five first clear sky MODIS images of NAFE'06, on JD 304, 308, 309, 310 and 311. Fig. 7 plots the areal average of 10 km resolution $\theta_{c,\text{MODIS}}$ as function of $1/r_{ah}$ (r_{ah} is computed from ground-based observation of wind speed). It appears that the model with default parameters $\gamma = 100$ s m^{-1} and $\theta_{c0} = 2.5\%$ v/v fits relatively well the observed mean $\theta_{c,\text{MODIS}}$, which justifies the assumptions made previously. A variation of 0.02 ms^{-1} in $1/r_{ah}$ (equivalent to 4.5 ms^{-1} in wind speed) induces an increase of 5% v/v in θ_c. For a given day, the spatial variability of θ_c within the SMOS pixel is about three times larger ($\sim 15\%$ v/v).

By fixing the value of γ to 100 s m^{-1}, one is able to estimate $\theta_{c0,\text{MODIS}}$ with Eq. (18) from fitted $\theta_{c,\text{MODIS}}$ and ground observations of r_{ah}

$$\theta_{c0,\text{MODIS}} = \frac{\theta_{c,\text{MODIS}}}{1 + \gamma/r_{ah}} \qquad (19)$$

The soil parameter $\theta_{c0,\text{MODIS}}$ is retrieved at 10 km resolution over the Yanco area and its sub-spatial variability (standard deviation) are mapped in Fig. 8. The spatial variability of $\theta_{c0,\text{MODIS}}$ is linked to soil type distribution. The soil in the near-surface over Yanco has a high clay content in the CIA (left part of the image) near Y9 and along the Yanco Creek (right part of the image) from Y5 to Y12, and a high sand content in the north of the Yanco area around Y2 (Hornbuckle and Christen, 1999; Merlin et al., 2007). To determine whether the retrieved θ_{c0} compensates for possible errors in MODIS derived soil temperature retrievals, it is correlated with MODIS NDVI at 10 km resolution. The correlation coefficient is 0.0004, which indicates that the retrieved θ_{c0} is mainly dependent on soil properties, and not on vegetation cover.

The downscaling schemes D1′ and D2′ are then applied to the NAFE'06 data set using the soil parameter $\theta_{c0,\text{MODIS}}$ retrieved from JD 304–311. Downscaling results are presented in Figs. 4 and 5 for each MODIS image separately. Quantitative results in terms of RMSE and correlation coefficient with L-band derived soil moisture are listed in Table 3, showing that the inclusion of a spatially variable θ_c in the

downscaling relationship significantly increases the accuracy of the disaggregation. The overall RMSE on the downscaled θ is decreased from 1.7% to 1.4% v/v with the linear approximation, and from 1.7% to 1.6% v/v with the second-order correction. The overall correlation coefficient is increased from 0.65 to 0.76 with the linear approximation and from 0.64 to 0.75 with the second-order correction. These improvements justify the relative complexity of D1′ compared to D1. However, the second-order correction in β^2 of D2 and D2′ does not improve the downscaling approach with this data set (and the β model used).

4.5. Uncertainties in fractional vegetation cover

The performance of disaggregation approaches depends on fractional vegetation cover estimates. The uncertainties in f_{veg} can be associated with uncertainties in NDVI$_{\text{min}}$ and NDVI$_{\text{max}}$. The NDVI value at full vegetation cover NDVI$_{\text{max}}$ is not very accurate in the low-covered NAFE'06 area, and the value for NDVI$_{\text{min}}$ (0.22) does not probably correspond to pixels with 100% bare soil. To assess the impact of uncertainties in fractional vegetation cover on disaggregation results, a sensitivity analysis was conducted by adding a bias of $\pm$ 0.1 to NDVI$_{\text{min}}$ and NDVI$_{\text{max}}$. Results in terms of RMSE on disaggregated soil moisture are presented in Table 4 for downscaling algorithms D1 and D1′. When looking at the results for D1, a bias on

Table 4
Sensitivity of the disaggregation algorithms D1 and D1′ to a bias of ±0.1 on extreme NDVI values

Bias (–)		RMSE (% v/v) on	
NDVI$_{\text{min}}$	NDVI$_{\text{max}}$	θ_{D1}	$\theta_{\text{D1}'}$
0	0	1.69	1.45
0	+0.1	1.70	1.43
0	−0.1	1.75	1.44
+0.1	0	2.03	1.41
+0.1	+0.1	2.03	1.41
+0.1	−0.1	2.03	1.41
−0.1	0	1.84	1.43
−0.1	+0.1	1.73	1.46
−0.1	−0.1	2.14	1.43

The RMSE on disaggregated soil moisture is computed from data including all days except JD 307.

NDVI$_{min}$ has in general more impact than a bias on NDVI$_{max}$. This was expected as most pixels are in the lower range of NDVI values. In the worst case (negative bias on both NDVI$_{min}$ and NDVI$_{max}$), the overall RMSE on disaggregated soil moisture is estimated as 2.1% v/v, which is relatively small compared to the range of variation of 10 km resolution soil moisture (0–15% v/v). When looking at the results for D1', it is apparent that a bias on vegetation fraction estimates has almost no effect on disaggregation results. In fact, the errors associated with an under(or over)estimation of f_{veg} is compensated by the calibration of θ_{c0}. Consequently, the sensitivity study indicates that the impact of uncertainties in extreme NDVI values is relatively small, and can be corrected by a calibration strategy. Moreover, it should be noted that the accuracy of NDVI$_{max}$ can potentially be improved by combining the maximum NDVI value observed within the study area with the value extrapolated along the dry edge of the temperature-NDVI triangle.
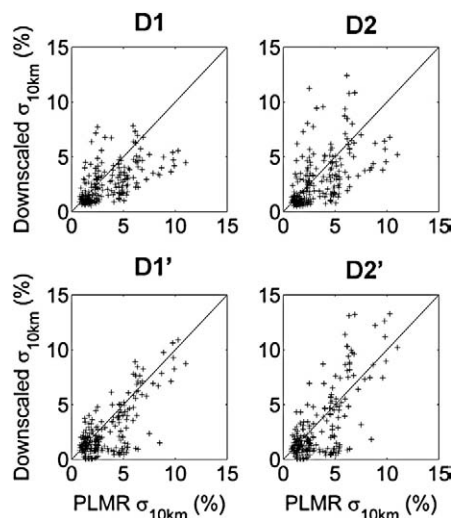
4.6. Observation time

The disaggregation results obtained separately with MODIS aboard Terra (10 am) and MODIS aboard Aqua (1 pm) are compared in Table 3. While the RMSE is about the same with Terra and with Aqua for all downscaling schemes, the mean correlation coefficient between the downscaled and PLMR derived soil moisture varies between 0.57 and 0.68 with Terra data and between 0.72 and 0.84 with Aqua data depending on the downscaling scheme. The downscaling approaches appear to be generally more robust with Aqua than with Terra, despite the interpolation of PLMR data on three days out of the six clear sky images (JD 310, 312 and 321). Actually, the acquisition time of surface temperature is an important requirement for β estimation, as the evaporation process directly depends on incoming solar radiation. These results confirm that the coupling between optical derived β and near-surface soil moisture is generally stronger at 1 pm than at 10 am.

4.7. Noise-level reduction at 10 km resolution

In the disaggregation approaches, the MODIS soil temperature was aggregated from 1 to 10 km to reduce the noise-level in data. The aim here is to verify the noise reduction at 10 km resolution under certain conditions. Table 5 lists the 10 km variability in the SMOS pixel and the 1 km variability in 10 km fields of successively, NDVI, soil skin temperature, SMP, disaggregated soil moisture (scheme D1'), and PLMR derived soil moisture. When looking at the dry down period JD 308–310 following the first rainfall event, it appears that the 1 km variability of SMP increases on JD 309 from 0.23–0.24 to 0.38, while the 10 km resolution variability is constant at 0.18–0.19. By assuming that the spatial variability of soil moisture generally decreases with the mean during a dry down period (Teuling et al., 2007), it can be

Fig. 9. 1 km variability in 10 km fields ($\sigma_{10\ km}$) of downscaled soil moisture versus the $\sigma_{10\ km}$ of PLMR derived soil moisture (for all acquisition dates except JD 307).

concluded that i) the noise-level in SMP observation is higher on JD 309 than on the other days, and ii) the aggregation to 10 km reduces significantly random errors at 1 km resolution. Note that the higher uncertainty in SMP on JD 309 is probably due to the observation time: the data on JD 309 were acquired at 10 am aboard Terra, while the data on JD 308 and 310 were acquired at 1 pm aboard Aqua.

4.8. Robustness at 10 km resolution

The robustness of the downscaling schemes is assessed by plotting in Fig. 9 the 1 km variability in 10 km fields ($\sigma_{10\ km}$) of downscaled soil moisture versus the $\sigma_{10\ km}$ of PLMR derived soil moisture. The RMSE (and correlation coefficient) is 1.9% (0.61), 2.1% (0.58), 1.8% (0.73), and 2.1% v/v (0.72) for D1, D2, D1'$_{\wedge}$ and D2'$_{\wedge}$ respectively. Results indicate that D1'$_{\wedge}$ is the most stable of the four approaches. Moreover, the RMSE on the $\sigma_{10\ km}$ of downscaled soil moisture (1.8% v/v for D1'$_{\wedge}$) is about twice as small as the mean $\sigma_{10\ km}$ of PLMR derived soil moisture (3.4% v/v). This means that the spatial variability of near-surface soil moisture is relatively well represented below the scale of 10 km. The scale of the disaggregation algorithm could therefore be improved to a resolution higher than 10 km. However, further studies are needed to estimate quantitatively an "optimal" downscaling resolution in between the MODIS resolution (1 km) and 10 km.

5. Discussion

Comparison of the algorithms using soil properties at SMOS scale θ_{cSMOS} and at the disaggregation scale $\theta_{c,MODIS}$ shows that parameter θ_c is the most important parameter to be estimated at both high- and low-resolution. The application of the methodology to SMOS would therefore require estimating θ_c over large areas. Given the correlation between θ_c and sand/clay fraction (Komatsu, 2003), this parameter could possibly be derived from existing soil maps. However, soil maps of the first cm of soil are not available globally and consequently a more robust approach is to estimate θ_c from remote sensing observations. One way to do this would be to use the temporal behaviour of near-surface soil moisture observation as an index of soil evaporative rate: for a given surface area with approximately the same amount of precipitation, the faster the soil dries, the higher θ_c is. An iterative procedure on $\theta_{c,MODIS}$ is proposed. First, the SMOS-scale $\theta_{c,SMOS}$ is estimated from a time series of SMOS observation θ_{SMOS} and SMOS-scale β_{SMOS}. Next, $\theta_{c,MODIS}$ is initialized $\theta_{c,MODIS}=\theta_{c,SMOS}$, and is retrieved at improved spatial resolution (10 km or higher), by iteratively (i) downscaling θ_{SMOS} and (ii) evaluating $\theta_{c,MODIS}$ from the

Table 5
10 km variability in the SMOS pixel and 1 km variability in 10 km fields of successively, NDVI, soil temperature, SMP (Soil Moisture Proxy), disaggregated soil moisture (scheme D1'$_{\wedge}$) and PLMR derived soil moisture

		10 km variability in the SMOS pixel (1 km variability in 10 km fields)				
		σNDVI	σT_{MODIS}	σSMP$_{MODIS}$	$\sigma\theta_{D1'}$	$\sigma\theta_{PLMR}$
Day	Satellite	–	K	–	% v/v	% v/v
304	Aqua	0.033 (0.041)	1.0 (1.6)	0.17 (0.25)	1.9 (2.3)	2.7 (3.2)
307	Terra	idem	2.2 (2.3)	0.39 (0.36)	6.5 (5.4)	2.0 (4.7)
308	Aqua	idem	1.5 (1.9)	**0.18 (0.23)**	2.7 (2.6)	2.2 (3.7)
309	Terra	idem	0.76 (1.4)	**0.18 (0.38)**	1.7 (3.0)	2.3 (3.4)
310	Aqua	idem	1.4 (1.9)	**0.19 (0.24)**	2.3 (2.4)	2.4 (3.3)
311	Terra	idem	1.3 (2.0)	0.14 (0.25)	2.2 (2.8)	2.3 (3.1)
312	Aqua	idem	1.7 (1.9)	0.24 (0.26)	2.9 (2.5)	2.3 (3.1)
313	Terra	idem	1.1 (1.6)	0.14 (0.21)	1.9 (2.4)	2.1 (2.9)
313	Aqua	idem	1.1 (1.8)	0.15 (0.26)	1.2 (1.7)	2.1 (2.9)
318	Terra	idem	1.0 (1.4)	0.15 (0.23)	1.7 (2.2)	1.7 (3.2)
321	Aqua	idem	1.5 (1.7)	0.26 (0.34)	2.0 (2.3)	2.3 (3.3)
322	Terra	idem	1.2 (1.7)	0.18 (0.26)	1.7 (2.3)	2.4 (3.4)

dowsncaled θ and measured β_{MODIS} (in Eq. (18)). Such a downscaling/assimilation coupling scheme would combine the spatial pattern search (downscaling) and the temporal dynamics search (assimilation) in an optimal manner (Merlin et al., 2006a).

The main limitation of the general downscaling approach outlined in this paper is the derivation of accurate SMP (or soil evaporative efficiency) estimates. For NAFE'06, the LAI ranged from 0 to 1.5 at 1 km resolution, resulting in relatively low fractional vegetation covers. It should be noted that the uncertainty in soil skin temperature retrievals increases with LAI, and the retrieval will not be feasible over fully vegetated pixels. Also, the formulation of the fractional vegetation cover f_{veg} as a linear function of NDVI in Eq. (3) could be improved (Baret et al., 2007). A second limitation of the method is estimation of the minimum soil temperature T_{min}, as it partly depends on a subjective interpretation of the triangle. As depicted by Carlson (2007) "the most severe limitation of the triangle method is that identification of the triangular shape in the pixel distribution requires a flat surface and a large number of pixels over an area with a wide range of soil wetness and fractional vegetation cover". However, the downscaling approach differs from the traditional triangle analysis as it does not require estimating the maximum soil temperature T_{max}. As T_{max} can be largely uncertain, especially after a rainfall event when the soil is wet everywhere in the SMOS pixel, the use of SMP (instead of soil evaporative efficiency) represents a key step in the downscaling procedures. One drawback of the use of SMP is that the denominator ($T_{MODIS} - T_{min}$) is subject to numerical instabilities when the MODIS derived soil temperature is close to the minimum soil temperature.

6. Summary and conclusions

A deterministic approach for downscaling ~40 km resolution SMOS soil moisture observations was developed from 1 km resolution MODIS data. To account for the lower soil moisture sensitivity of MODIS surface temperature compared to L-band brightness temperature, the downscaling scale was fixed to 10 times (10 km) the spatial resolution of MODIS thermal data (1 km). The three general steps of the downscaling procedure were (i) estimate soil evaporative efficiency from MODIS data (ii) link soil evaporative efficiency to near-surface soil moisture via a physically-based scaling function and (iii) build a downscaling relationship to express high-resolution near-surface soil moisture as function of SMOS type observation and high-resolution soil evaporative efficiency. This innovative approach was able to account for spatial variations in soil type and temporal variations in wind speed and near-soil moisture across the SMOS pixels. Four different downscaling algorithms were proposed. They differed only with regards to i) the assumed relationship (linear or nonlinear) between soil evaporative efficiency and near-surface soil moisture, and ii) the scale at which soil parameters (θ_c) were available (40 km or 10 km).

The four downscaling algorithms have been tested using the NAFE'06 data set. The 1 km resolution L-band derived soil moisture was aggregated over the Yanco area to generate a time series of coarse-scale (~40 km) near-surface soil moisture observations. The simulated SMOS soil moisture was then disaggregated by the different downscaling algorithms. The disaggregation results obtained at 10 km resolution from twelve MODIS surface temperature images (six aboard Terra and six aboard Aqua) were compared with the L-band derived soil moisture aggregated to 10 km.

The overall root mean square difference between downscaled and L-band derived soil moisture was better than 1.8% v/v with soil moisture values ranging from 0 to 15% v/v. The consistency between downscaled and L-band derived soil moisture was also demonstrated at the 1 km scale. The overall RMSE on sub-pixel variability (standard deviation within 10 km resolution pixels) of downscaled soil moisture was better than 2.1% v/v with a variability ranging from 0 to 12% v/v. In all cases, the correlation coefficient between downscaled and L-band derived soil moisture (and its sub-pixel variability) was better than 0.6. These results illustrated the remarkable robustness of the four different algorithms at 10 km resolution across the three-week experiment. It was found that results are more accurate with MODIS/Aqua than with MODIS/Terra data, due to the stronger coupling between β and near-surface soil moisture at 1 pm than at 10 am.

The comparison of the linear and non-linear algorithms showed that better results were generally obtained with the linear approximation. It was argued that the aggregation from 1 km to 10 km of MODIS-derived soil temperature and L-band derived soil moisture tends to "linearize" the correlation between soil evaporative efficiency and near-surface soil moisture around the SMOS observation. However, as the soil moisture variability over the study area was mainly due to irrigation at scales smaller than 1 km, it is not possible to generalize this finding to SMOS pixels with a stronger heterogeneity at 10 km resolution, for which the impact of the non-linearity of β would be higher.

The comparison of the algorithms using soil properties at the SMOS scale $\theta_{c,SMOS}$ and at the disaggregation scale $\theta_{c,MODIS}$ showed that θ_c is the most important parameter to be estimated at both high- and low-resolution. The knowledge of θ_c at 10 km resolution made the overall RMSE on downscaled soil moisture decrease from 1.7% v/v to 1.3% v/v, and the mean correlation coefficient increase from 0.7 to 0.8.

The application to SMOS data would imply coupling the disaggregation approach with an assimilation scheme in order to retrieve soil parameters (e.g. θ_c) at the disaggregation scale. Further testing will be needed to assess the applicability of such an approach in a wider range of surface conditions, especially over higher vegetation covers. Also, studies evaluating the relative sensitivity of L-band observations and soil moisture proxies (such as soil evaporative efficiency) are needed to determine optimal disaggregation scales in terms of downscaling accuracy.

References

Anderson, M. C., Norman, J. M., Mecikalski, J. R., Otkin, J. A., & Kustas, W. P. (2007). A climatological study of evapotranspiration and moisture stress across the continental united states based on thermal remote sensing: 2. surface moisture climatology. *Journal of Geophysical Research*, 112(D11112).

Baret, F., Hagolle, O., Geiger, B., Bicheron, P., Miras, B., Huc, M., Berthelot, B., Nino, F., Weiss, M., Samain, O., Roujean, J. L., & Leroy, M. (2007). LAI, fA-PAR and fCover CYCLOPES global products derived from VEGETATION—Part 1: Principles of the algorithm. *Remote Sensing of Environment*, 110, 275–286.

Carlson, T. (2007). An overview of the 'triangle method' for estimating surface evapotranspiration and soil moisture from satellite imagery. *Sensors*, 7, 1612–1629.

Carlson, T. N., Gillies, R. R., & Schmugge, T. J. (1995). An interpretation of methodologies for indirect measurement of soil water content. *Agricultural and Forest Meteorology*, 77, 191–205.

Chauhan, N. S., Miller, S., & Ardanuy, P. (2003). Spaceborne soil moisture estimation at high resolution: a microwave-optical/IR synergistic approach. *International Journal of Remote Sensing*, 24(22), 4599–4622.

Crago, R., & Brutsaert, W. (1996). Daytime evaporation and the self-preservation of the evaporative fraction during the daytime. *Journal of Hydrology*, 178, 241–255.

Crow, W. T., & Zhan, X. (2007). Continental-scale evaluation of remotely sensed soil moisture products. *IEEE Geoscience and Remote Sensing Letters*, 4(3), 451–455.

Gentine, P., Entekhabi, D., Chehbouni, A., Boulet, G., & Duchemin, B. (2007). Analysis of evaporative fraction diurnal behaviour. *Agricultural and Forest Meteorology*, 143, 13–29.

Hornbuckle, J. W., & Christen, E. (1999). Physical properties of soils in the Murrumbidgee and Colembally irrigation areas. *CSIRO Land and Water Technical Report*, vol. 17/99.

Kerr, Y. H. (2007). Soil moisture from space: where are we? *Hydrogeology Journal*, 15, 117–120.

Kerr, Y. H., Waldteufel, P., Wigneron, J.-P., Martinuzzi, J.-M., Font, J., & Berger, M. (2001). Soil moisture retrieval from space: the soil moisture and ocean salinity (SMOS) mission. *IEEE Transactions on Geoscience and Remote Sensing*, 39, 1729–1735.

Komatsu, T. S. (2003). Towards a robust phenomenological expression of evaporation efficiency for unsaturated soil surfaces. *Journal of Applied Meteorology*, 42, 1330–1334.

Lhomme, J. P., & Elguero, E. (1999). Examination of the evaporative fraction diurnal behaviour using a soil–vegetation model coupled with a mixed-layer model. *Hydrology and Earth System Sciences*, 3(2), 259–270.

Liu, S., Mao, D., & Jia, L. (2007). Evaluating parameterizations of aerodynamic resistance to heat transfer using field measurements. *Hydrology and Earth System Sciences*, 11, 769–783.

Merlin, O., Chehbouni, G., Boulet, G., & Kerr, Y. (2006). Assimilation of disaggregated microwave soil moisture into a hydrologic model using coarse-scale meterological data. *Journal of Hydrometeorology*, 7, 1308–1322.

Merlin, O., Chehbouni, G., Kerr, Y., & Goodrich, D. (2006). A downscaling method for distributing surface soil moisture within a microwave pixel: Application to the Monsoon'90 data. *Remote Sensing of Environment*, 101, 379–389.

Merlin, O., Chehbouni, G., Walker, J. P., Panciera, R., & Kerr, Y. (2008). A simple method to disaggregate passive microwave based soil moisture. *IEEE Transactions on Geoscience and Remote Sensing*, 46(3). doi:10.1109/TGRS.2007.914807 SMOS Special Issue.

Merlin, O., Walker, J. P., Kalma, J. D., Kim, E. J., Hacker, J., Panciera, R., Young, R., Summerell, G., Hornbuckle, J., Hafeez, M., & Jackson, T. J. (2008). The NAFE'06 data set: towards soil moisture retrieval at intermediate resolution. *Advances in Water Resources*. doi:10.1016/j.advwatres.2008.01.018.

Merlin, O., Walker, J., Panciera, R., Young, R., Kalma, J., & Kim, E. (2007). Soil moisture measurement in heterogeneous terrain. *MODSIM 2007 International Congress on Modelling and Simulation* (pp. 2604–2610). New Zealand: Modelling and Simulation Society of Australia and New Zealand.

Merlin, O., Walker, J.P., Panciera, R., Escorihuela, M.J., Jackson, T.J., Submitted for publication. Assessing the SMOS soil moisture retrieval parameters with high-resolution NAFE'06 data. Geosci. and Remote Sens. Lett.

Nichols, W. E., & Cuenca, R. H. (1993). Evaluation of the evaporative fraction for parameterization of the surface. *Water Resour. Res.*, 29(11), 3681–3690.

Nishida, K., Nemani, R. R., Glassy, J. M., & Running, S. W. (2003). Development of an evapotranspiration index from Aqua/MODIS for monitoring surface moisture status. *IEEE Transactions on Geoscience and Remote Sensing*, 41(2), 493–501.

Price, J. C. (1980). The potential of remotely sensed thermal infrared data to infer surface soil moisture and evaporation. *Water Resources Research*, 16, 787–795.

Prigent, C., Aires, F., Rossow, W. B., & Robock, A. (2005). Sensitivity of satellite microwave and infrared observations to soil moisture at a global scale: Relationship of satellite observations to in situ soil moisture measurements. *Journal of Geophysical Research*, 110(D07110).

Sellers, P. J., Heiser, M. D., & Hall, F. G. (1992). Relations between surface conductance and spectral vegetation indices at intermediate (100 m² to 15 km²) length scales. *Journal of Geophysical Research*, 97(D17), 19033–19059.

Shuttleworth, W. J., Gurney, R. J., Hsu, A. Y., & Ormsby, J. P. (1989). FIFE: the variation in energy partition at surface flux sites. *IAHS Publication*, 186, 67–74.

Shuttleworth, W. J., Yang, Z.-L., & Arain, M. A. (1997). Aggregation rules for surface parameters in global models. *Hydrology and Earth System Sciences*, 2, 217–226.

Teuling, A. J., Uijlenhoet, R., Hurkmans, R., Merlin, O., Panciera, R., Walker, J., & Troch, P. A. (2007). Dry-end surface soil moisture variability during NAFE'06. *Geophysical Research Letters*, 34(L17402). doi:10.1029/2007GL031001.

Wagner, W., Bloschl, G., Pampaloni, P., Calvet, J.-C., Bizzari, B., Wigneron, J.-P., & Kerr, Y. (2007). Operational readiness of microwave remote sensing of soil moisture for hydrologic applications. *Nordic hydrology*, 38(1), 1–20.